Progress In Electromagnetics Research B, Vol. 26, 361–382, 2010

RELIABLE SIMULATION-DRIVEN DESIGN OPTIMIZATION OF MICROWAVE STRUCTURES USING MANIFOLD MAPPING

S. Koziel

Engineering Optimization & Modeling Center
School of Science and Engineering
Reykjavik University, Menntavegur 1, 101 Reykjavik, Iceland

D. Echeverría Ciaurri

Department of Energy Resources Engineering
School of Earth Sciences
Stanford University, Stanford, CA 94305, USA

Abstract—A computationally efficient surrogate-based framework for reliable simulation-driven design optimization of microwave structures is described. The key component of our algorithm is manifold mapping, a response correction technique that aligns the coarse model (computationally cheap representation of the structure under consideration) with the accurate but CPU-intensive (fine) model of the optimized device. The parameters of the manifold mapping surrogate are explicitly calculated based on the fine model data accumulated during the optimization process. Also, manifold mapping does not use any extractable parameters, which makes it easy to implement. Robustness and excellent convergence properties of the proposed algorithm are demonstrated through the design of several microwave devices including microstrip filters and a planar antenna.

1. INTRODUCTION

Electromagnetic (EM) simulation-driven design and design optimization becomes increasingly important in contemporary microwave engineering. The primary reason is that due to a growing complexity of

Received 2 September 2010, Accepted 25 October 2010, Scheduled 2 November 2010
Corresponding author: koziel@ru.is (koziel@ru.is).

microwave structures it is more and more difficult to carry out the design process using analytical models. Also, no systematic procedures exist for many emerging classes of structures (e.g., ultra-wideband antennas [1] or substrate integrated circuits [2]) that would be able to yield designs satisfying given specification requirements. In all these cases, EM-simulation-based design may be the only option. On the other hand, using a full-wave EM solver directly in the optimization loop is usually prohibitive because of high computational cost. A possible workaround to this is co-simulation [3–5], where the EM model is broken down into smaller parts that are combined with circuit components in a circuit simulator. Although this approach reduces the evaluation time for a single design, the EM-embedded co-simulation model is still subjected to computationally heavy direct EM-driven optimization.

Computationally efficient design optimization of microwave structures can be realized by replacing the CPU-intensive fine model with a low-cost but less accurate surrogate model. Space mapping (SM) [6–17], tuning procedures [18–22], as well as various response correction methods [23, 24] are examples of very efficient approaches of this kind used in microwave engineering.

Space mapping utilizes the surrogate model constructed from a computationally cheap coarse model [6, 15] combined with auxiliary transformations to reduce misalignment between the surrogate and the fine model. Parameters of these transformations are obtained by solving a separate nonlinear regression problem. The coarse model is normally a physics-based model. This type of models has typically a larger validity region than approximation/interpolation models. For that reason, preferred coarse model choices in microwave applications are, for example, equivalent circuits or models built on analytical formulas; in some cases, EM models resulting from a coarse grid discretization can also be used although these models are often not exempt from some computational cost, and therefore have to be used economically. Space mapping usually yields satisfactory designs after a few fine model evaluations; however, its performance depends heavily on the quality of the coarse model considered and on the proper selection of the type of transformations used for the surrogate [25].

Simulation-based tuning [22] exploits the circuit-theory-based tunable components that are embedded in an EM simulator through internal ports created in the underlying model [20]. The tuning model thus created can be optimized very efficiently. We stress that this methodology is invasive regarding the simulator used, and hence, in most situations cannot be applied in a straightforward manner. Additionally, it is not clear if tuning can be directly applicable for

radiating structures (antennas). Various combinations of tuning and space mapping have also been reported in the literature [26–28].

In this paper, a manifold-mapping (MM) technique [29, 30] is applied to simulation-driven design of microwave structures. Manifold mapping can be considered as a response correction method that utilizes available fine model data to align the coarse and fine model responses not only at the current design but also at a number of points previously considered in the optimization. In that sense, manifold mapping can be viewed as a generalization of the output SM concept [10]. However, the MM surrogate model is conceptually different than the output SM one. More specifically, while the output SM correction term is simply a difference between the fine and surrogate model responses at the current design (so that zero-order consistency is ensured [31]), the MM model aims at a first-order agreement. In order to improve the convergence properties of the manifold mapping algorithm and its overall performance, a few modifications with respect to the basic formulation in [29] are introduced. Efficiency and robustness of the presented technique is demonstrated through the design of several microwave devices including microstrip filters and a planar antenna.

2. MICROWAVE DESIGN OPTIMIZATION THROUGH MANIFOLD MAPPING

In this section, we formulate the microwave design problem, recall the basics of the manifold-mapping technique, and compare this technique with other similar approaches, namely, space mapping. We also describe modifications introduced to the basic MM algorithm that improve its robustness.

2.1. Design Problem Formulation

Let $\mathbf{R_f}(\mathbf{x}) \in R^m$ denote the response vector of a fine model of the microwave structure of interest (e.g., $|S_{21}|$ evaluated at m different frequencies), $\mathbf{x} \in R^n$ be a vector of design variables (e.g., structure dimensions), and U be a given objective function, e.g., minimax. We want to solve the following problem

$$\mathbf{x_f^*} = \arg\min_{\mathbf{x}} \mathrm{U}\left(\mathbf{R_f}(\mathbf{x})\right). \tag{1}$$

The fine model is assumed to be computationally expensive, typically obtained by a time-consuming EM simulation, so that the direct solving of (1), for example, by a gradient-based optimizer with numerical derivatives, is prohibitive. It should be also noticed that

the solution $\mathbf{x}_\mathbf{f}^*$ is a local optimizer, and that global approaches within simulation-based optimization are not in general practically feasible.

2.2. Manifold-mapping Optimization Algorithm

Manifold mapping relies on the existence of the coarse model response $\mathbf{R_c}(\mathbf{x};\mathbf{r}) \in R^m$, faster to evaluate than the fine model response, but less accurate. The (local) misalignment between the fine and coarse model responses can be reduced by means of the calibration parameters $\mathbf{r} \in R^r$ that are, in principle, different to the design variables $\mathbf{x}$. Thus, the fine model optimizer $\mathbf{x}_\mathbf{f}^*$ can be approximated by

$$\mathbf{x}_\mathbf{c}^*(\mathbf{r}) = \arg\min_{\mathbf{x}} \mathrm{U}\left(\mathbf{R_c}(\mathbf{x};\mathbf{r})\right). \tag{2}$$

The coarse model response could be aligned, for example, around the optimization initial guess $\mathbf{x}^{(0)} \in R^n$

$$\mathbf{r}_{\mathbf{x}^{(0)}}^* = \arg\min_{\mathbf{r}} \left\| \mathbf{R_f}\left(\mathbf{x}^{(0)}\right) - \mathbf{R_c}\left(\mathbf{x}^{(0)};\mathbf{r}\right) \right\|. \tag{3}$$

The point $\mathbf{x}_\mathbf{c}^*(\mathbf{r}_{\mathbf{x}^{(0)}}^*)$ may yield a better approximation of the fine model optimizer.

In many practical cases, the design accuracy given by $\mathbf{x}_\mathbf{c}^*(\mathbf{r}_{\mathbf{x}^{(0)}}^*)$ is not satisfactory. However, a local model response correction in the neighbourhood of this point leads quite often to better solutions at the expense of only a few additional fine model simulations.

Manifold mapping [29] exploits a surrogate-based optimization (SBO) scheme [10] and can be formulated as

$$\mathbf{x}^{(i+1)}(\mathbf{r}) = \arg\min_{\mathbf{x}} \mathrm{U}\left(\mathbf{R}_\mathbf{s}^{(i)}(\mathbf{x};\mathbf{r})\right), \tag{4}$$

where $\mathbf{R}_\mathbf{s}^{(i)}(\mathbf{x};\mathbf{r}) \in R^m$ is a surrogate model response at iteration i. (For a clearer notation and unless needed, from now on we will omit the dependence of the model responses and solutions on the calibration parameters $\mathbf{r}$.)

The manifold-mapping surrogate model is defined as

$$\mathbf{R}_\mathbf{s}^{(i)}(\mathbf{x}) = \mathbf{R_f}\left(\mathbf{x}^{(i)}\right) + \mathbf{S}^{(i)}\left(\mathbf{R_c}(\mathbf{x}) - \mathbf{R_c}\left(\mathbf{x}^{(i)}\right)\right), \tag{5}$$

with $\mathbf{S}^{(i)}$ being the $m \times m$ linear correction (matrix) defined as

$$\mathbf{S}^{(i)} = \mathbf{\Delta F}\mathbf{\Delta C}^\dagger, \tag{6}$$

where

$$\mathbf{\Delta F} = \left[\mathbf{R_f}\left(\mathbf{x}^{(i)}\right) - \mathbf{R_f}\left(\mathbf{x}^{(i-1)}\right) \quad \ldots \quad \mathbf{R_f}\left(\mathbf{x}^{(i)}\right) - \mathbf{R_f}\left(\mathbf{x}^{\max\{i-n,0\}}\right)\right] \tag{7}$$

$$\mathbf{\Delta C} = \left[\mathbf{R_c}\left(\mathbf{x}^{(i)}\right) - \mathbf{R_c}\left(\mathbf{x}^{(i-1)}\right) \quad \ldots \quad \mathbf{R_c}\left(\mathbf{x}^{(i)}\right) - \mathbf{R_c}\left(\mathbf{x}^{\max\{i-n,0\}}\right)\right]. \tag{8}$$

Here, † denotes the pseudoinverse operator defined as

$$\mathbf{\Delta C}^{\dagger} = \mathbf{V}_{\mathbf{\Delta C}} \mathbf{\Sigma}^{\dagger}_{\mathbf{\Delta C}} \mathbf{U}_{\mathbf{\Delta C}}, \tag{9}$$

where $\mathbf{U}_{\mathbf{\Delta C}}$, $\mathbf{\Sigma}_{\mathbf{\Delta C}}$, and $\mathbf{V}_{\mathbf{\Delta C}}$ are the factors in the singular value decomposition of $\mathbf{\Delta C}$. The matrix $\mathbf{\Sigma}^{\dagger}_{\mathbf{\Delta C}}$ is the result of inverting the nonzero entries in $\mathbf{\Sigma}_{\mathbf{\Delta C}}$, leaving the zeroes invariant [29]. Notice that the manifold-mapping surrogate model has in our applications a similar computational complexity than the coarse model (all the final model responses have been obtained previously).

The correction term $\mathbf{S}^{(i)}$ is an approximation of the "ideal" manifold mapping that is defined as

$$\mathbf{R_s}(\mathbf{x}) = \mathbf{R_f}(\mathbf{x_f^*}) + \mathbf{S}(\mathbf{R_c}(\mathbf{x}) - \mathbf{R_c}(\mathbf{x_f^*})), \tag{10}$$

with

$$\mathbf{S} = \mathbf{J_f}(\mathbf{x_f^*})\,\mathbf{J_c^{\dagger}}(\mathbf{x_f^*}), \tag{11}$$

where $\mathbf{J_f}(\mathbf{x_f^*})$ and $\mathbf{J_c}(\mathbf{x_f^*})$ stand for the fine and coarse model Jacobians at $\mathbf{x_f^*}$, respectively. Obviously, neither $\mathbf{x_f^*}$ nor $\mathbf{S}$ is known beforehand. Therefore one needs to use the approximation (6) in the actual algorithm. The "ideal" manifold-mapping model alignment is

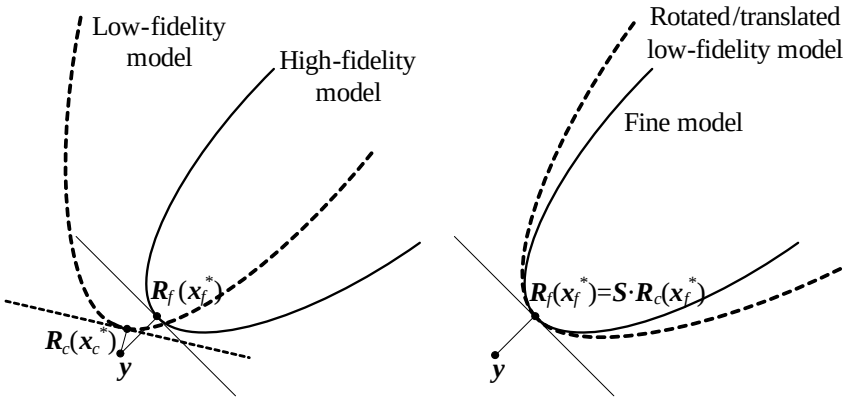

Figure 1. Illustration of the manifold-mapping model alignment for a least-squares optimization problem: $\mathbf{x_f^*}$ and $\mathbf{x_c^*}$ denote the optimal solutions associated to $\mathbf{R_f}$ and $\mathbf{R_c}$, respectively, and $\mathbf{y}$ are the design specifications given. Thin solid and dashed straight lines denote the tangent planes for the fine and coarse model at their optimal designs, respectively. By the linear correction $\mathbf{S}$, the point $\mathbf{R_c}(\mathbf{x_c^*})$ is mapped to $\mathbf{R_f}(\mathbf{x_f^*})$, and the tangent plane for $\mathbf{R_c}$ at $\mathbf{R_c}(\mathbf{x_c^*})$ to the tangent plane for $\mathbf{R_f}$ at $\mathbf{R_f}(\mathbf{x_f^*})$ [29].

illustrated in Fig. 1 for a least-squares optimization problem

$$\mathbf{U}\left(\mathbf{R_f}\left(\mathbf{x}\right)\right) = ||\mathbf{R_f}\left(\mathbf{x}\right) - \mathbf{y}||_2^2, \tag{12}$$

with $\mathbf{y} \in R^m$ being the design specifications given.

In this work, $\mathbf{S}^{(i)}$ is set to be the identity matrix during the first n iterations (i.e., while $i < n$). This appears to stabilize the MM algorithm in its early stages.

It is important to know that if the coarse model has a negligible computational cost when compared to the fine model, the objective function in (4) can be explored globally. The MM algorithm is in this case endowed with some robustness with respect to multiple local minima in (1).

For least-squares optimization problems, manifold mapping is supported by mathematically sound convergence theory [46]. We can identify four factors relevant for the convergence of the scheme above to the fine model optimizer $\mathbf{x_f^*}$:

1) the model responses being smooth;
2) the coarse model optimization in (2) being well-posed;
3) the discrepancy of the optimal model response $\mathbf{R_f}\left(\mathbf{x_f^*}\right)$ with respect to the design specification being small enough;
4) and the coarse model response being a sufficiently good approximation of the fine model response.

In most practical situations the requirements associated to the first three factors are satisfied, and since the coarse models considered in those cases are very often based on expert knowledge accumulated over the years, the similarity between the fine and model responses is high enough for having convergence of the manifold-mapping algorithm.

The results in [46] rely mainly on the smoothness of the model responses involved. Therefore, we can expect convergence of the manifold-mapping algorithm for a cost function U smooth enough. When U is not differentiable, we have so far the experimental evidence given in this work for the applicability of manifold mapping to designs based on minimax objective functions. Since the manifold mapping is between model responses, it makes sense that the methodology yields satisfactory solutions even when U is not smooth.

The basic manifold-mapping algorithm given below can be modified in a number of ways. Model sensitivities appear to improve basic convergence if derivative information is framed within Generalized Manifold Mapping [47]. The incorporation of a Levenberg-Marquardt strategy in manifold mapping [30, 47] can be seen as a convergence safeguard analogous to trust-region methods [48]. Manifold mapping can also be extended to designs where the

constraints are determined by time-consuming functions, and where these constraints can be dealt with in a multi-level approach [46].

The following features make the manifold-mapping algorithm an attractive alternative to other surrogate-based methods used in microwave engineering so far:

- The manifold-mapping algorithm does not include a parameter extraction step because the surrogate model correction is explicitly calculated using available fine/coarse model data. This makes MM simpler and easier to implement.
- The manifold-mapping surrogate model (5) is uniquely determined. In the case of the general space-mapping algorithm, there are a large number of options available, and a good algorithm performance depends on a careful, and not always straightforward, selection.
- Upon convergence the surrogate model satisfies (asymptotically) both zero- and first-order consistency conditions [31] with respect to the fine model. This allows for a more accurate computation of the fine model optimum $\mathbf{x}_\mathbf{f}^*$.

2.3. Coarse Model Preconditioning and Adaptive Search Radius

In order to improve the performance of the manifold mapping algorithm, the coarse model can be (initially) preconditioned as in (3), taking advantage of the calibration parameters $\mathbf{r}$. This space-mapping-like alignment process aims at reducing the discrepancy between the fine and coarse model responses.

While the calibration parameters might be any parameters traditionally used by space mapping [6], in this work we only use so-called preassigned parameters exploited by implicit space mapping [10]. In case of microwave devices these might be, for example, substrate parameters such as height or the dielectric constant value. Note that the alignment process is only performed once (at the initial design), and therefore, it does not increase significantly the computational complexity of the optimization process.

In order to improve the convergence properties of the MM algorithm, the surrogate model optimization step (4) is replaced by a constrained version

$$\mathbf{x}^{(i+1)} = \underset{||\mathbf{x}_{\min}^{(i)} - \mathbf{x}|| \leq \delta^{(i)}}{\arg\min} \; \mathrm{U}\left(\mathbf{R}_\mathbf{s}^{(i)}(\mathbf{x})\right) \tag{13}$$

where $\mathbf{x}_{\min}^{(i)}$ is the solution vector prior to $\mathbf{x}^{(i)}$ with lowest cost function, and $\delta^{(i)}$ is the search radius. The update $\delta^{(i)}$ follows a heuristic

strategy inspired in the trust-region approach [48] that appears to work adequately in our applications. If the two most recent iterations yield improvement in the objective function, the search radius is increased. The search radius is reduced if the current iteration does not improve the fine model objective function, and remains unchanged otherwise. Unlike in the trust-region space-mapping approach [15], in this scheme no solutions are rejected. This allows incorporating all available fine model data in constructing a (hopefully) better surrogate model.

The search radius $\delta^{(i)}$ is updated as follows ($\delta^{(0)}$ and $\alpha,\ \beta > 1$ are user defined arguments; in our numerical experiments we use $\alpha = 2$ and $\beta = 3$):

if $\left(U\left(\mathbf{R_f}\left(\mathbf{x}^{(i+1)}\right)\right) < U\left(\mathbf{R_f}\left(\mathbf{x}^{(i)}_{\min}\right)\right)\right) \wedge \left(U\left(\mathbf{R_f}\left(\mathbf{x}^{(i)}\right)\right) < U\left(\mathbf{R_f}\left(\mathbf{x}^{i-1}\right)\right)\right)$

$\quad \delta^{(i+1)} = \alpha\delta^{(i)}$

else if $U\left(\mathbf{R_f}\left(\mathbf{x}^{(i+1)}\right)\right) > U\left(\mathbf{R_f}\left(\mathbf{x}^{(i)}\right)\right)$

$\quad \delta^{(i+1)} = \delta^{(i)} \Big/ \beta$

else

$\quad \delta^{(i+1)} = \delta^{(i)}$

end

2.4. Design Optimization Procedure

Figure 2 shows the flowchart of our design optimization procedure exploiting manifold mapping, coarse model preconditioning and adaptive adjustment of the surrogate model search radius. Note that the fine model is evaluated only once per iteration. Most of the operations are performed on the manifold mapping surrogate model, which is computationally cheap, so that the total optimization cost is essentially determined by the fine model evaluation time.

2.5. Manifold Mapping Optimization with Function Approximation Coarse Model

As mentioned in the introduction, the preferred coarse model choices are equivalent circuits or models exploiting analytical formulas. Such models are sufficiently fast to avoid excessive computational overhead due to numerous evaluations while performing surrogate model optimization. For many structures, however, reliable equivalent-circuit or analytical models are not available. These include, among others, ultrawideband antennas, substrate integrated circuits as well as various waveguide structures.

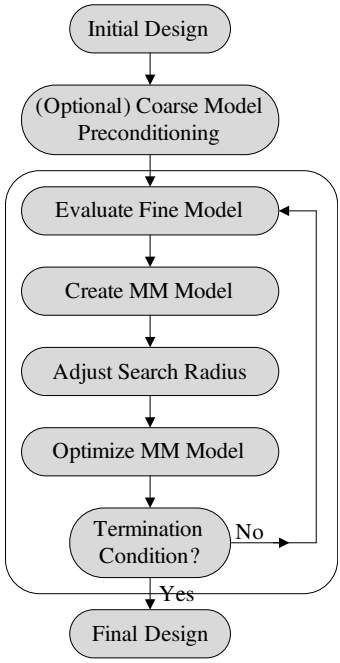

Figure 2. Flowchart of the manifold-mapping-based optimization procedure. Coarse model preconditioning (3) is optional. Each iteration of the MM algorithm consists of fine model evaluation (only once per iteration), construction of the MM surrogate model (5)–(9), adaptive adjustment of the search radius (cf. Section 2.3), as well as the surrogate model optimization (13) that yields a new design. The termination condition used in this work is $\|\mathbf{x}^{(i)} - \mathbf{x}^{(i-1)}\| < 10^{-4}$.

A generic coarse model that is always available is a coarse-discretization EM model exploiting the same electromagnetic solver as the one used to implement the fine model. Unfortunately, such model is normally computationally too expensive to be used directly in the SM- or MM-based optimization process.

A feasible alternative is to build the coarse model through function approximation of the coarse-discretization EM-simulation data. The model created this way is computationally cheap. Moreover, if the design space is sampled in a sufficiently dense way, the model is able to inherit good generalization properties from its coarse-discretization EM "original". This creates a practical problem though: given the sampling density, the number of samples grows exponentially with the number of design variables and may become impracticably large

even for 5 or 6 design variables. Therefore, it is recommended to perform the optimization process in two stages [32]: (i) find the approximation optimum of the coarse-discretization EM model, (ii) set up a function approximation coarse model only in the neighbourhood of this optimum.

The procedure for setting up the function approximation coarse model can be then summarized as follows:

1. Find approximate optimum $\mathbf{x}^*_{\mathbf{cd}}$ of the coarse-discretization EM model $\mathbf{R}_{\mathbf{cd}}$;
2. Determine the neighbourhood $X^*_{\mathbf{cd}}$ of $\mathbf{x}^*_{\mathbf{cd}}$ where the coarse model will be established (this step can be performed using sensitivity analysis);
3. Allocate $N_{\mathbf{cd}}$ samples in $X^*_{\mathbf{cd}}$ and obtain the coarse-dicretization EM model data (design of experiments can be performed using, e.g., Latin Hypercube Sampling [33]);
4. Create the coarse model by approximating coarse-discretization EM model data (using, e.g., RBF interpolation [34], kriging [35], support vector regression [36, 37], etc.).

An example of exploiting this procedure can be found in Section 3.4, where the coarse model is constructed using kriging interpolation.

3. VERIFICATION EXAMPLES

In this section, several examples of MM-based design optimization are given for verification purposes, including three microstrip filters and a planar UWB antenna. We illustrate good convergence properties as well as overall performance of the proposed technique. In all cases, satisfactory designs are obtained at the computational cost corresponding to several evaluations of the fine model.

3.1. Miniature Dual-mode Bandpass Microstrip Filter [38]

Consider the miniature dual-mode bandpass filter [38] shown in Fig. 3. The design parameters are $\mathbf{x} = [L\ s\ p\ g]^T$; $W = 1\,\text{mm}$, $W_c = 0.5\,\text{mm}$. The fine model is simulated in FEKO [39]. The coarse model is the circuit model implemented in Agilent ADS [40] (Fig. 4). The design specifications are $|S_{21}| \geq -1\,\text{dB}$ for $2.35\,\text{GHz} \leq \omega \leq 2.45\,\text{GHz}$, $|S_{21}| \leq -20\,\text{dB}$ for $1.6\,\text{GHz} \leq \omega \leq 2.2\,\text{GHz}$ and for $2.6\,\text{GHz} \leq \omega \leq 3.2\,\text{GHz}$. The initial design is $\mathbf{x}^{(0)} = [12.0\ 0.905\ 1.273\ 0.185]^T\,\text{mm}$ (optimum of $\mathbf{R}_{\mathbf{c}}$).

The coarse model was preconditioned as in (3) using substrate height and dielectric constants corresponding to microstrip models of

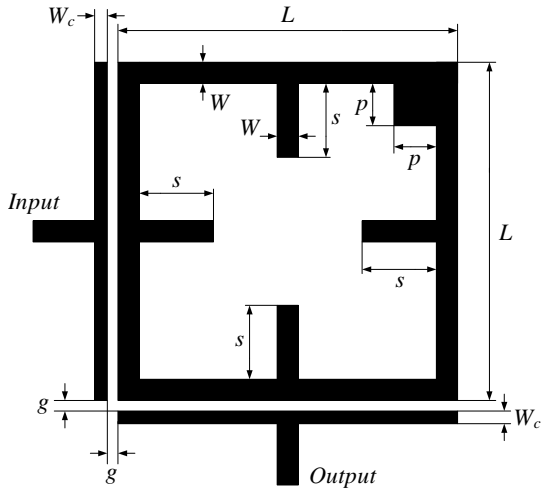

Figure 3. Miniature dual-mode bandpass filter: geometry [38].

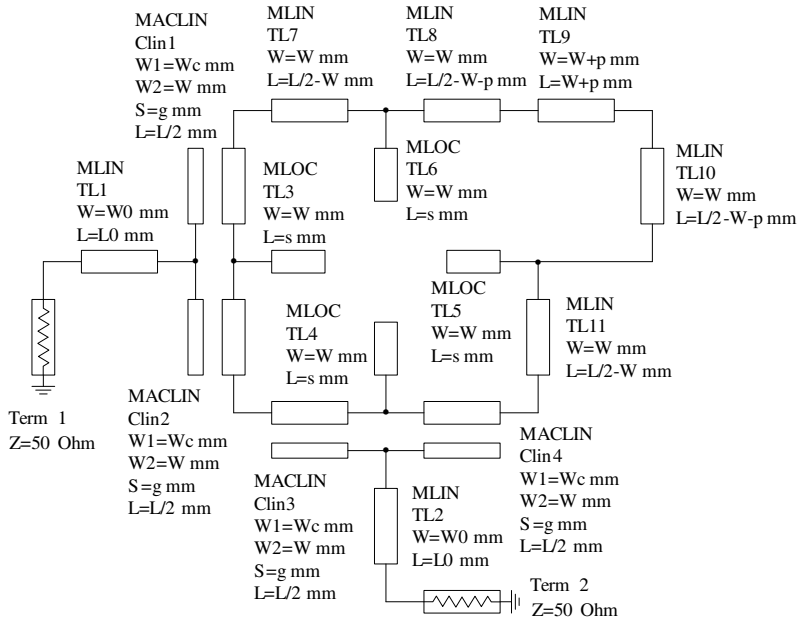

Figure 4. Miniature dual-mode bandpass filter: coarse model (Agilent ADS).

the equivalent circuit as preassigned parameters. The MM algorithm yields an optimized design $\mathbf{x}^* = [13.143\ 0.792\ 1.466\ 0.1285]^T$ mm with the corresponding specification error of −0.45 dB (Fig. 5). It should be emphasized that the MM algorithm exhibits a very consistent convergence pattern as shown in Fig. 6. The optimization cost is 13 fine model evaluations (termination condition was set to $\|\mathbf{x}^{(i)} - \mathbf{x}^{(i-1)}\| < 10^{-4}$). The cost of coarse/surrogate model operations can be neglected (evaluation time for $\mathbf{R_c}$ is a small fraction of a second versus about 15 minutes for $\mathbf{R_f}$).

For the sake of comparison, the filter was also optimized using pattern search [49]. The quality of the design obtained with pattern search is similar to that found by the MM algorithm (specification error −0.44 dB), however, computational cost is substantially higher (114 fine model evaluations). Optimization using Matlab's *fmincon* [50] failed to find a design satisfying the specifications (the best design

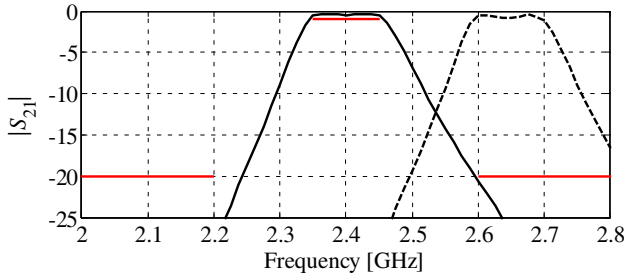

Figure 5. Miniature dual-mode bandpass filter: Initial (dashed line) and optimized (solid line) $|S_{21}|$ versus frequency; optimized design obtained using MM algorithm. Design specifications are denoted using horizontal lines.

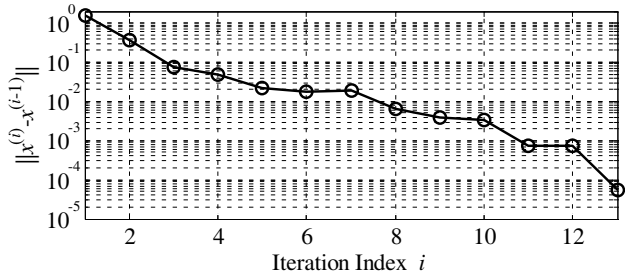

Figure 6. Miniature dual-mode bandpass filter: convergence plot. Iteration index coincides with the number of fine model evaluations.

obtained after 150 fine model evaluations was still violating the specifications by 0.1 dB).

3.2. Wideband Bandstop Microstrip Filter [41]

Consider the wideband bandstop microstrip filter [41] shown in Fig. 7(a). The design parameters are $\mathbf{x} = [L_r\ W_r\ L_c\ W_c\ G_c]^T$. The fine model $\mathbf{R_f}$ is simulated in FEKO [39]. The coarse model $\mathbf{R_c}$ is the circuit model implemented in Agilent ADS [40] (Fig. 7(b)). The design

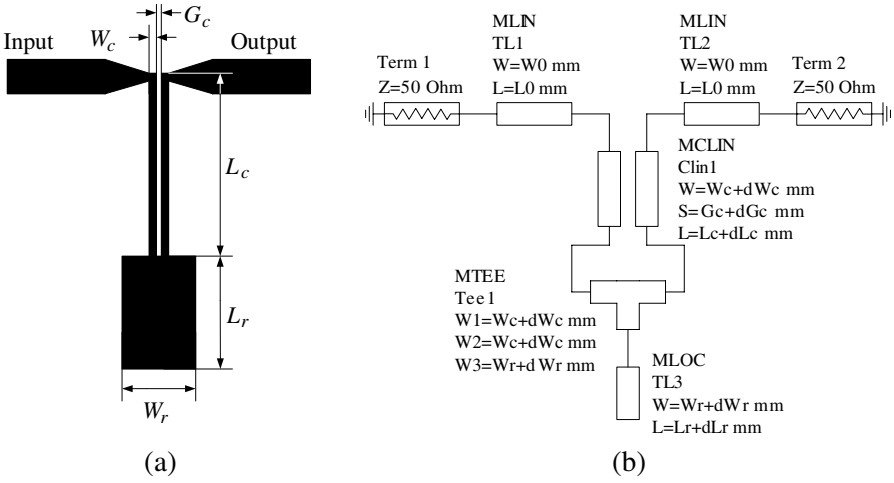

Figure 7. Wideband bandstop microstrip filter: (a) geometry [41], (b) coarse model (Agilent ADS).

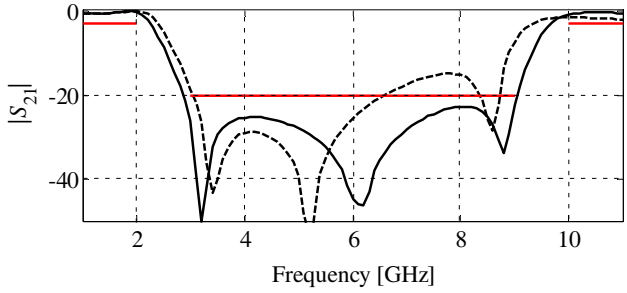

Figure 8. Wideband bandstop filter: Initial (dashed line) and optimized (solid line) $|S_{21}|$ versus frequency; optimized design obtained using MM algorithm. Design specifications are denoted using horizontal lines.

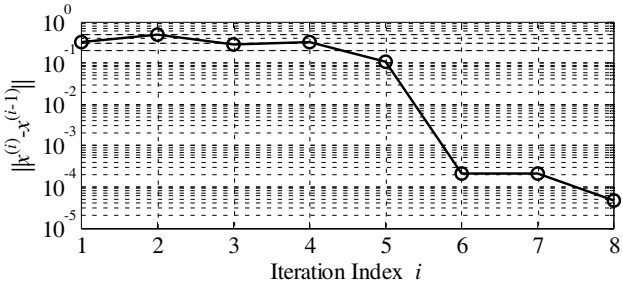

Figure 9. Wideband bandstop filter: convergence plot. Iteration index coincides with the number of fine model evaluations.

specifications are $|S_{21}| \geq -3\,\text{dB}$ for $1.0\,\text{GHz} \leq \omega \leq 2.0\,\text{GHz}$, $|S_{21}| \leq -20\,\text{dB}$ for $3.0\,\text{GHz} \leq \omega \leq 9.0\,\text{GHz}$, and $|S_{21}| \geq -3\,\text{dB}$ for $10.0\,\text{GHz} \leq \omega \leq 11.0\,\text{GHz}$. The initial design is $x^{(0)} = [7\ 1\ 9\ 0.1\ 0.1]^T$ mm.

As in the previous example, $\mathbf{R}_c$ was preconditioned by adjusting the values of the substrate heights and dielectric constants of the microstrip components Clin1 and TL3 (Fig. 7(b)). The MM optimization algorithm yields an optimized design $\mathbf{x}^* = [7.15\ 1.199\ 8.20\ 0.05\ 0.1296]^T$ mm (Fig. 8) with the corresponding specification error of −2.3 dB. Fig. 9 shows the convergence plot. The optimization cost is only 9 fine model evaluations (termination condition $\|\mathbf{x}^{(i)} - \mathbf{x}^{(i-1)}\| < 10^{-4}$).

3.3. Wideband Ring Resonator Bandpass Filter [42]

Our third example is the wideband ring resonator bandpass filter [42] shown in Fig. 10. The design parameters are $\mathbf{x} = [L_1\ L_2\ L_3\ W_1\ W_2\ S]^T$ mm. The fine model is simulated in FEKO [39]. The coarse model (Fig. 11) is implemented in Agilent ADS [40]. The design specifications are $|S_{21}| \geq -1\,\text{dB}$ for $3.0\ \text{GHz} \leq \omega \leq 5.5\,\text{GHz}$, and $|S_{21}| \leq -20\,\text{dB}$ for $2.0\,\text{GHz} \leq \omega \leq 2.7\,\text{GHz}$ and $5.8\,\text{GHz} \leq \omega \leq 6.5\,\text{GHz}$. The initial design is the coarse model optimal solution $\mathbf{x}^{(0)} = [6.803\ 6.179\ 4.598\ 0.615\ 0.050\ 0.159]^T$ mm (specification error +23.6 dB).

Again, the coarse model was preconditioned using (3). The optimized design found by the manifold mapping algorithm is $\mathbf{x}^* = [6.672\ 6.042\ 4.253\ 0.621\ 0.05\ 0.171]^T$ (specification error −0.52 dB), Fig. 12. Fig. 13 shows the convergence plot. The optimization cost is only 10 fine model evaluations (termination condition $\|\mathbf{x}^{(i)} - \mathbf{x}^{(i-1)}\| < 10^{-4}$).

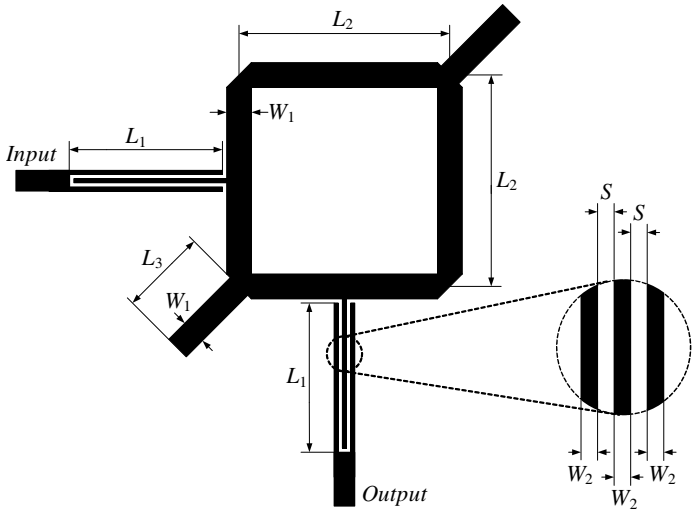

Figure 10. Wideband ring resonator bandpass filter: geometry [42].

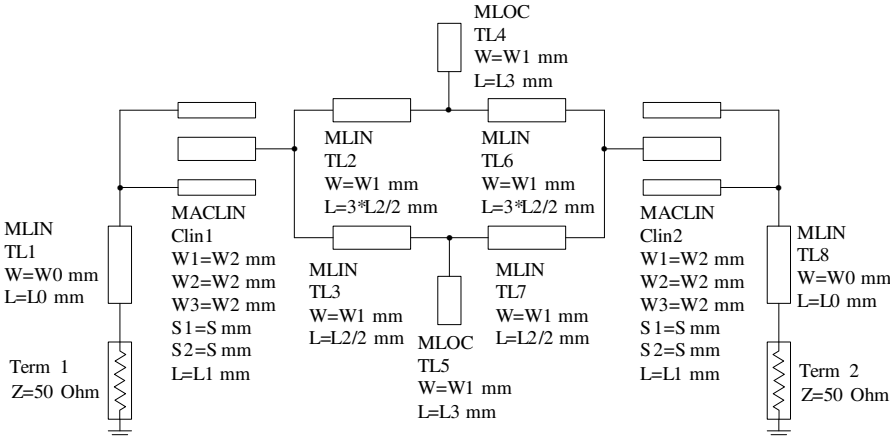

Figure 11. Wideband ring resonator bandpass filter: coarse model (Agilent ADS).

3.4. UWB Planar Dipole Antenna

Our last example is the planar dipole antenna shown in Fig. 14, consisting of the main radiator element and two parasitic strips [43]. The design variables are $\mathbf{x} = [l_0\ w_0\ a_0\ l_p\ w_p\ s_0]^T$. Other variables are: $a_1 = 0.5\,\text{mm}$, $w_1 = 0.5\,\text{mm}$. Rogers RT5880 laminate is used for

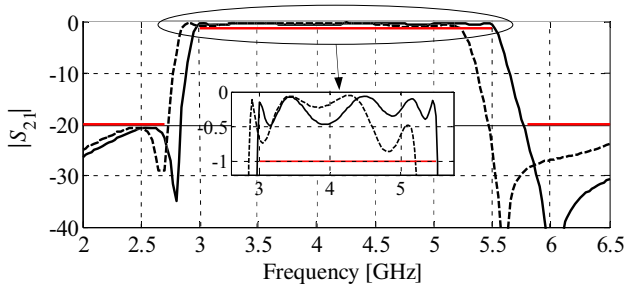

Figure 12. Wideband ring resonator filter: Initial (dashed line) and optimized (solid line) $|S_{21}|$ versus frequency; optimized design yielded by MM algorithm. Design specifications are denoted using horizontal lines.

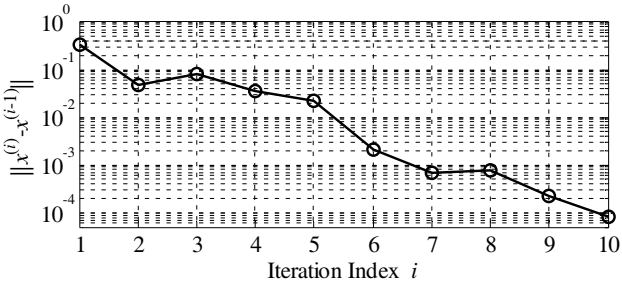

Figure 13. Wideband ring resonator bandpass filter: convergence plot. Iteration index coincides with the number of fine model evaluations.

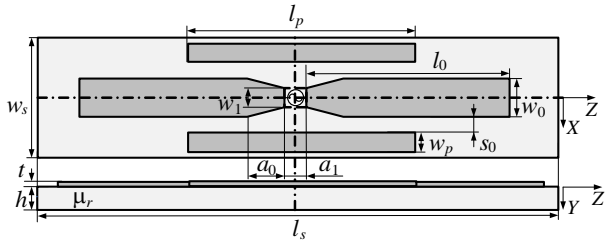

Figure 14. Dipole antenna geometry [43]: top and side views. The dash-dot lines show the magnetic (YOZ) and the electric (XOY) symmetry walls. The 50 ohm source impedance is not shown at the figure.

the substrate dielectric, the substrate height is $h = 1.58$ mm. The fine model $\mathbf{R_f}$ of the antenna structure (10,250,412 mesh cells at the initial design, evaluation time 44 minutes) is simulated using the CST MWS transient solver [44]. The design objective is to obtain $|S_{11}| \leq -10$ dB for 3.1 GHz to 10.6 GHz. The initial design is $\mathbf{x}^{(0)} = [20\ 10\ 1\ 10\ 8\ 2]^T$ mm.

Because no reliable circuit equivalent is available, we use the coarse-discretization models: $\mathbf{R_{cd}}$ (108,732 mesh cells at $\mathbf{x}^{(0)}$, evaluation time 43 seconds). This model is too expensive to be used directly in the manifold-mapping optimization process. Therefore, we build a kriging-interpolation-based coarse model $\mathbf{R_c}$ exploiting the methodology described in Section 2.5. In the first stage, we find the approximate optimum of $\mathbf{R_{cd}}$, $\mathbf{x}^*_{\mathbf{cd}} = [18.66\ 12.98\ 0.526\ 13.717\ 8.00\ 1.094]^T$ mm. The computational cost of this step is 127 evaluations of $\mathbf{R_{cd}}$ (which corresponds to about two evaluations of the fine model). The kriging-based coarse model is constructed in the neighbourhood $X^*_{\mathbf{cd}}$ of $\mathbf{x}^*_{\mathbf{cd}}$ determined by the lower and upper bounds $\mathbf{x}^*_{\mathbf{cd}} - \boldsymbol{\delta}$ and $\mathbf{x}^*_{\mathbf{cd}} + \boldsymbol{\delta}$, where $\boldsymbol{\delta} = [0.5\ 0.5\ 0.2\ 0.5\ 1.5\ 0.2]^T$ mm (the region size was determined based on the coarse-discretization model sensitivity). We use $N_{\mathbf{cd}} = 100$ samples allocated using Latin Hypercube Sampling [33]. To set up the coarse model we exploit Matlab kriging toolbox DACE [45].

Figure 15 shows the responses of the fine model at the initial design $\mathbf{x}^{(0)}$ (specification error +3.3 dB), at the optimal design of the coarse-discretization model $\mathbf{R_{cd}}$ (specification error −1.3 dB) and at the final design obtained using the manifold-mapping algorithm its optimized design $\mathbf{x}^* = [19.1478\ 12.9434\ 0.3278\ 13.8905\ 6.7683\ 1.0874]^T$ mm

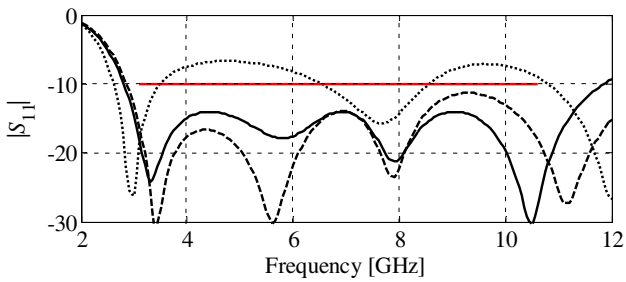

Figure 15. Dipole antenna: $|S_{11}|$ versus frequency at initial design (dotted line), coarse-discretization model optimum (dashed line) and the optimized design obtained using MM algorithm (solid line). Design specifications are denoted using horizontal lines.

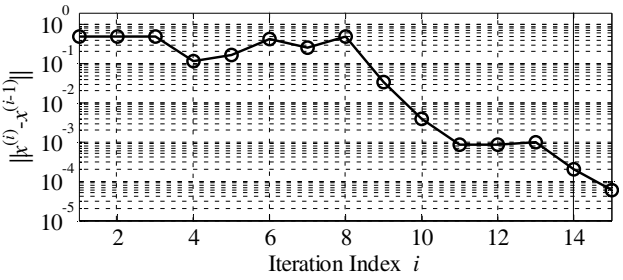

Figure 16. Dipole antenna: convergence plot. Iteration index coincides with the number of fine model evaluations.

(specification error −4.1 dB). Figure 16 shows the convergence plot. The optimization cost is 15 fine model evaluations (the termination condition is $\|\mathbf{x}^{(i)} - \mathbf{x}^{(i-1)}\| < 10^{-4}$).

4. CONCLUSION

A robust and computationally efficient design optimization procedure exploiting a manifold mapping algorithm is presented. Our technique is easy to implement. Interaction between the coarse and fine model is simplified because the surrogate model can be constructed using explicit formulas (there is no need to extract model parameters by solving a nonlinear regression problem). The robustness of our approach is demonstrated through the design optimization of several microstrip filters and a UWB planar antenna.

ACKNOWLEDGMENT

This work was supported in part by the Reykjavik University Development Fund under Grant T10006. The authors thank Agilent Technologies, Santa Rosa, CA, for making ADS available, and CST AG, Darmstadt, Germany, for making CST Microwave Studio available.

REFERENCES

1. Schantz, H., *The Art and Science of Ultrawideband Antennas*, Artech House, 2005.
2. Wu, K., "Substrate integrated circuits (SiCs) — A new paradigm

for future GHz and THz electronic and photonic systems," *IEEE Circuits and Systems Society Newsletter*, Vol. 3, No. 2, Apr. 2009.

3. Rizzoli, V., A. Costanzo, D. Masotti, and P. Spadoni, "Circuit-level nonlinear/electromagnetic co-simulation of an entire microwave link," *IEEE MTT-S Int. Microwave Symp. Dig.*, 813–816, Long Beach, CA, Jun. 2005.
4. Shin, S. and S. Kanamaluru, "Diplexer design using EM and circuit simulation techniques," *IEEE Microwave Magazine*, Vol. 8, No. 2, 77–82, Apr. 2007.
5. Snyder, R. V., "Practical aspects of microwave filter development," *IEEE Microwave Magazine*, Vol. 8, No. 2, 42–54, Apr. 2007.
6. Bandler, J. W., Q. S. Cheng, S. A. Dakroury, A. S. Mohamed, M. H. Bakr, K. Madsen, and J. Søndergaard, "Space mapping: The state of the art," *IEEE Trans. Microwave Theory Tech.*, Vol. 52, No. 1, 337–361, Jan. 2004.
7. Ismail, M. A., D. Smith, A. Panariello, Y. Wang, and M. Yu, "EM-based design of large-scale dielectric-resonator filters and multiplexers by space mapping," *IEEE Trans. Microwave Theory Tech.*, Vol. 52, No. 1, 386–392, Jan. 2004.
8. Wu, K.-L., Y.-J. Zhao, J. Wang, and M. K. K. Cheng, "An effective dynamic coarse model for optimization design of LTCC RF circuits with aggressive space mapping," *IEEE Trans. Microwave Theory Tech.*, Vol. 52, No. 1, 393–402, Jan. 2004.
9. Rayas-Sánchez, J. E., F. Lara-Rojo, and E. Martínez-Guerrero, "A linear inverse space mapping (LISM) algorithm to design linear and nonlinear RF and microwave circuits," *IEEE Trans. Microwave Theory Tech.*, Vol. 53, No. 3, 960–968, Mar. 2005.
10. Koziel, S., J. W. Bandler, and K. Madsen, "A space mapping framework for engineering optimization: Theory and implementation," *IEEE Trans. Microwave Theory Tech.*, Vol. 54, No. 10, 3721–3730, Oct. 2006.
11. Dorica, M. and D. D. Giannacopoulos, "Response surface space mapping for electromagnetic optimization," *IEEE Trans. Magn.*, Vol. 42, No. 4, 1123–1126, Apr. 2006.
12. Amari, S., C. LeDrew, and W. Menzel, "Space-mapping optimization of planar coupled-resonator microwave filters," *IEEE Trans. Microwave Theory Tech.*, Vol. 54, No. 5, 2153–2159, May 2006.
13. Crevecoeur, G., L. Dupre, and R. van de Walle, "Space mapping optimization of the magnetic circuit of electrical machines

including local material degradation," *IEEE Trans. Magn.*, Vol. 43, No. 6, 2609–2611, Jun. 2007.

14. Pantoja, M. F., P. Meincke, and A. R. Bretones, "A hybrid genetic-algorithm space-mapping tool for the optimization of antennas," *IEEE Trans. on Antennas and Propagation*, Vol. 55, No. 3, Part 1, 777–781, Mar. 2007.
15. Koziel, S., Q. S. Cheng, and J. W. Bandler, "Space mapping," *IEEE Microwave Magazine*, Vol. 9, No. 6, 105–122, Dec. 2008.
16. Crevecoeur, G., P. Sergeant, L. Dupre, and R. van de Walle, "Two-level response and parameter mapping optimization for magnetic shielding," *IEEE Trans. Magn.*, Vol. 44, No. 2, 301–308, Feb. 2008.
17. Sergeant, P., R. V. Sabariego, G. Crevecoeur, L. Dupre, and C. Geuzaine, "Analysis of perforated magnetic shields for electric power applications," *IET Electric Power Applications*, Vol. 3, No. 2, 123–132, Mar. 2009.
18. Rautio, J. C., "RF design closure — Companion modeling and tuning methods," *IEEE MTT IMS Workshop: Microwave Component Design Using Space Mapping Technology*, San Francisco, CA, 2006.
19. Swanson, D. G. and R. J. Wenzel, "Fast analysis and optimization of combline filters using FEM," *IEEE MTT-S IMS Digest*, 1159–1162, Boston, MA, Jul. 2001.
20. Rautio, J. C., "EM-component-based design of planar circuits," *IEEE Microwave Magazine*, Vol. 8, No. 4, 79–90, Aug. 2007.
21. Swanson, D. and G. Macchiarella, "Microwave filter design by synthesis and optimization," *IEEE Microwave Magazine*, Vol. 8, No. 2, 55–69, Apr. 2007.
22. Rautio, J. C., "Perfectly calibrated internal ports in EM analysis of planar circuits," *IEEE MTT-S Int. Microwave Symp. Dig.*, 1373–1376, Atlanta, GA, Jun. 2008.
23. Koziel, S., J. W. Bandler, and K. Madsen, "Space mapping with adaptive response correction for microwave design optimization," *IEEE Trans. Microwave Theory Tech.*, Vol. 57, No. 2, 478–486, 2009.
24. Koziel, S., "Efficient optimization of microwave circuits using shape-preserving response prediction," *IEEE MTT-S Int. Microwave Symp. Dig*, 1569–1572, Boston, MA, 2009.
25. Koziel, S., J. W. Bandler, and K. Madsen, "Quality assessment of coarse models and surrogates for space mapping optimization," *Optimization and Engineering*, Vol. 9, No. 4, 375–391, 2008.

26. Meng, J., S. Koziel, J. W. Bandler, M. H. Bakr, and Q. S. Cheng, "Tuning space mapping: A novel technique for engineering design optimization," *IEEE MTT-S Int. Microwave Symp. Dig.*, 991–994, Atlanta, GA, Jun. 2008.
27. Koziel, S., J. Meng, J. W. Bandler, M. H. Bakr, and Q. S. Cheng, "Accelerated microwave design optimization with tuning space mapping," *IEEE Trans. Microwave Theory Tech.*, Vol. 57, No. 2, 383–394, Feb. 2009.
28. Cheng, Q. S., J. W. Bandler, and S. Koziel, "Space mapping design framework exploiting tuning elements," *IEEE Trans. Microwave Theory and Tech.*, Vol. 58, No. 1, 136–144, 2010.
29. Echeverría, D. and P. W. Hemker, "Space mapping and defect correction," *CMAM Int. Mathematical Journal Computational Methods in Applied Mathematics,* Vol. 5, No. 2, 107–136, 2005.
30. Hemker, P. W. and D. Echeverría, "A trust-region strategy for manifold mapping optimization," *JCP Journal of Computational Physics*, Vol. 224, No. 1, 464–475, 2007.
31. Alexandrov, N. M. and R. M. Lewis, "An overview of first-order model management for engineering optimization," *Optimization Eng.*, Vol. 2, No. 4, 413–430, Dec. 2001.
32. Koziel, S., "Surrogate-based optimization of microwave structures using space mapping and kriging," *European Microwave Conference*, 1062–1065, Rome, Italy, Sep. 28–Oct. 2, 2009.
33. Beachkofski, B. and R. Grandhi, "Improved distributed hypercube sampling," *American Institute of Aeronautics and Astronautics*, 2002–1274, 2002.
34. Simpson, T. W., J. Peplinski, P. N. Koch, and J. K. Allen, "Metamodels for computer-based engineering design: Survey and recommendations," *Engineering with Computers*, Vol. 17, No. 2, 129–150, Jul. 2001.
35. Simpson, T. W., T. M. Maurey, J. J. Korte, and F. Mistree, "Kriging models for global approximation in simulation-based multidisciplinary design optimization," *American Institute of Aeronautics and Astronautic*, Vol. 39, No. 12, 2233–2241, Dec. 2001.
36. Yang, Y., S. M. Hu, and R. S. Chen, "A combination of FDTD and least-squares support vector machines for analysis of microwave integrated circuits," *Microwave Opt. Technol. Lett.*, Vol. 44, No. 3, 296–299, Feb. 2005.
37. Meng, J. and L. Xia, "Support-vector regression model for millimeter wave transition," *Int. J. Infrared and Milimeter Waves*,

Vol. 28, No. 5, 413–421, May 2007.

38. Lin, Y. F., C. H. Chen, K. Y. Chen, H. M. Chen, and K. L. Wong, "A miniature dual-mode bandpass filter using Al_2O_3 substrate," *IEEE Microw. Wireless Compon. Lett.*, Vol. 17, No. 8, 580–582, Aug. 2007.
39. FEKO® *User's Manual*, Suite 5.4, 2008, EM Software & Systems-S.A. (Pty) Ltd, 32 Techno Lane, Technopark, Stellenbosch, 7600, South Africa.
40. Agilent ADS, Version 2008, Agilent Technologies, 1400 Fountaingrove Parkway, Santa Rosa, CA 95403-1799, 2008.
41. Hsieh, M. Y. and S. M. Wang, "Compact and wideband microstrip bandstop filter," *IEEE Microwave and Wireless Component Lett.*, Vol. 15, No. 7, 472–474, Jul. 2005.
42. Sun, S. and L. Zhu, "Wideband microstrip ring resonator bandpass filters under multiple resonances," *IEEE Trans. Microwave Theory Tech.*, Vol. 55, No. 10, 2176–2182, Oct. 2007.
43. Spence, T. G. and D. H. Werner, "A novel miniature broadband/multiband antenna based on an end-loaded planar open-sleeve dipole," *IEEE Trans. Antennas Propag.,* Vol. 54, No. 12, 3614–3620, Dec. 2006.
44. CST Microwave Studio, Version 2009, CST AG, Bad Nauheimer Str. 19, D-64289 Darmstadt, Germany, 2009.
45. Lophaven, S. N., H. B. Nielsen, and J. Søndergaard, "DACE: A Matlab kriging toolbox," Technical University of Denmark, 2002.
46. Echeverría, D. and P. W. Hemker, "Manifold mapping: A two-level optimization technique," *Computing and Visualization in Science*, No. 11, 193–206, 2008.
47. Echeverría, D., "Two new variants of the manifold-mapping technique," *COMPEL the International Journal for Computation and Mathematics in Electrical Engineering*, Vol. 26, No. 2, 334–344, 2007.
48. Conn, A. R., N. Gould, and P. L. Toint, *Trust-region Methods*, MPS/SIAM Series on Optimization, SIAM, Philadelphia, 2007.
49. Kolda, T. G., R. M. Lewis, and V. Torczon, "Optimization by direct search: new perspectives on some classical and modern methods," *SIAM Review*, Vol. 45, No. 3, 385–482, 2003.
50. Matlab™, Version 7.6, The MathWorks, Inc., 3 Apple Hill Drive, Natick, MA 01760-2098, 2008.